

On the stability of persistent entropy and new summary functions for Topological Data Analysis

N. Atienza, R. Gonzalez Diaz, M. Soriano Trigueros

Department of Applied Mathematics I, University of Seville
{natiienza, rogo4i, msoriano4}@us.es

Abstract

Persistent homology and persistent entropy have recently become useful tools for pattern recognition. In this paper, we find requirements under which persistent entropy is stable to small perturbations in the input data and scale invariant. In addition, we describe two new stable summary functions combining persistent entropy and the Betti curve. Finally, we use the previously defined summary functions in a material classification task to show their usefulness in machine learning and pattern recognition.

1 Introduction

Topological data analysis (TDA) uses computational topology tools to study datasets. Intuitively, topological features like homology can be seen as qualitative geometric properties related to the notions of proximity and continuity and, therefore, can be useful tools for pattern recognition [1]. TDA has become a large field of research, with persistent homology (and its precursor known as size functions [2]) as its key tool. It has been applied successfully in many areas (see, for example, [3]). Its standard workflow is the following (see also Figure 1):

1. Start with a dataset, for example, a point cloud, endowed with some notion of proximity (usually a metric).
2. Depending on the kind of information we want to obtain, build a simplicial complex and a filter function on it. Compute a nested sequence of increasing subcomplexes (which encapsulate features from data) using the filter function.
3. Compute the homology of each subcomplex (intuitively, homology captures the “holes” of the underlying space) and study how it evolves in the sequence, leading to the key concept of persistent homology.

Persistent homology can be compactly represented using persistence barcodes [4], diagrams [5] and, more recently, landscapes [6]. There exist stability results showing that these representations are robust under small perturbations of the given data (see, for example, [7]). In addition, there are numerous software packages to calculate persistent homology and its representations. A nice study of the performance of available software packages is made in [8].

Although persistence barcodes, diagrams, and landscapes are metric spaces used to compare persistent homology of datasets, persistence barcodes and diagrams do not work properly for statistical analysis. For example, they fail to have unique mean (see [9]). Persistence landscapes perform better [6], but they are limited to the context of probability in Banach spaces. It is more useful sometimes to summarize the information contained in persistent homology using only a number. It becomes especially appropriate when only small samples are available since univariate non-parametric tests are required in these cases. Persistent entropy seems to be a perfect candidate to summarize persistent homology using only a number. Specifically, persistent entropy is the Shannon entropy [10] of a probability distribution obtained from persistent homology. It was defined in its current form in [11] but a precursor of this definition appears in [12]. Some successful applications of persistent entropy have been developed for pattern recognition of signals [13, 14], complex systems [15], biological images [16] and clustering [17]. A more theoretical approach allows persistent entropy to be used to distinguish topological features from noise [18]. With regards to

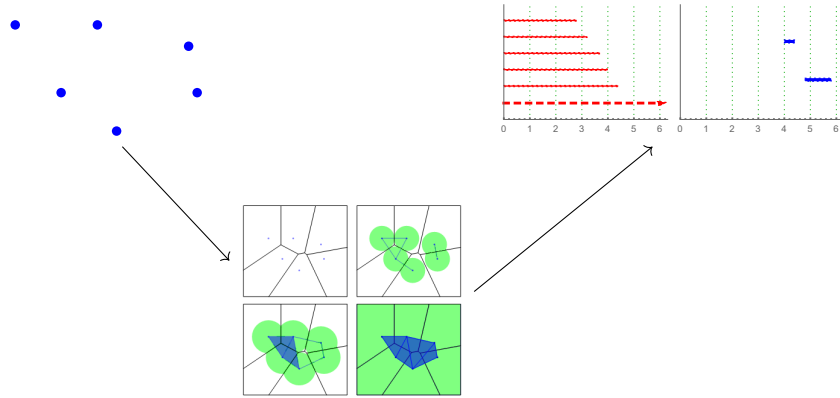


Figure 1: Standard workflow in topological data analysis.

implementation, persistent entropy has already been implemented as a method in Gudhi library¹, scikit-TDA library² and Giotto library³. Some partial results about stability of persistent entropy have been given in [14, 18] but, as far as we know, no formal study of persistent entropy has been done. The main objective of this paper is to provide a general stability result for persistent entropy and to study under which conditions persistent entropy is scale-invariant.

When it is not necessary to find significant differences in data but a classification task is needed, the usual approach is to replace statistical tests with machine learning methods. In this case, summarizing persistent homology in a number may be too restrictive, since we are projecting an infinite-dimensional space (persistence barcodes) to only one dimension (persistent entropy). One solution might be to use summary functions instead. Common approaches to summarizing persistence barcodes include kernel functions such as persistence multi-scale kernel [19], persistence weighted Gaussian kernel [20] and sliced Wasserstein kernel [21], as well as persistence-diagram vectorizations such as the already mentioned persistence landscape, persistence silhouettes [22], persistence images [23], Euler characteristic curves [24], topological intensity maps [25] and Betti curves [26, 27]. In this paper, we will define two new stable summary functions based on persistent entropy that can be used as a complementary function to the previous ones to describe persistence barcodes.

The paper is organized as follows. After recalling the theory of persistent homology in Section 2, stability and scale-invariance of persistent entropy is introduced in Section 3. In Section 4, we define two new summary functions derived from the concept of persistent entropy and study also their stability. Examples showing the applicability of these functions are also given. The usefulness of the summary functions defined in this paper is showed in Section 5. The paper ends with a section devoted to conclusions and future work.

2 Background

In this section, we give a quick overview of how algebraic topology is applied to data analysis. An instructive book showing the main algebraic topology tools for data analysis is [7].

As explained in the introduction, in order to apply algebraic topology tools to data analysis, we first must summarize the information provided by the data in a combinatorial structure, the simplicial complex structure being the most commonly used. Recall that an n -simplex is the convex hull of $n + 1$ affinely independent points. A 0-simplex is a point, a 1-simplex is a segment, a 2-simplex is a triangle, a 3-simplex is a tetrahedron and so on. A simplicial complex is a set of simplices glued in a specific way. An abstract simplicial complex can be seen as a way of storing the combinatorial structure of a simplicial complex.

¹ https://github.com/GUDHI/gudhi-devel/blob/master/src/python/gudhi/representations/vector_methods.py

² <https://github.com/scikit-tda/persim>

³ <https://github.com/giotto-ai/giotto-learn/blob/master/giotto/diagrams/features.py>

Definition 2.1 (abstract simplicial complex). Let X be a finite set. A family K of subsets of X is an abstract *simplicial complex* if for every subsets $\sigma \in K$ and $\sigma' \subseteq \sigma$, we have that $\sigma' \in K$ (in other words, non-empty intersections of simplices in K are also simplices of K). A subset in K of $m + 1$ elements of X is called an m -simplex.

When the finite set X represents data, the geometrical structure of its associated simplicial complex can provide information about how the data is related. Usually, these relations are not equally significant so it is common to define an order in its simplices to represent their importance. This can be done implicitly using a filter function.

Definition 2.2 (filtration). A *filter function* on a simplicial complex K is a monotonic function $f : K \rightarrow \mathbb{R}$ satisfying that $\sigma' \subset \sigma$ implies $f(\sigma') \leq f(\sigma)$. A *filtration* on K , obtained from f , is the sequence of subcomplexes $(K_t)_{t \in \mathbb{R}}$ where $K_t = f^{-1}(-\infty, t]$.

Notice that, because of the monotonicity of f , the set K_t is a simplicial complex for all t , and $t_1 < t_2$ implies that $K_{t_1} \subseteq K_{t_2}$. To help intuition, the parameter t will be referred as *time* although its physical meaning may be completely different. The following definition is an example of filtration and requires X to be a metric space.

Definition 2.3 (Vietoris-Rips filtration). Let X be a finite set of points endowed with a distance d_X . The Vietoris-Rips filtration of X is the sequence $(Rips(X, t))_{t \in \mathbb{R}}$ obtained from the filter function

$$f([x_0, \dots, x_m]) = \max_{0 \leq i, j \leq m} d_X(x_i, x_j)$$

where, for each $t \in \mathbb{R}$, the simplices of the Vietoris-Rips simplicial complex $Rips(X, t)$ are defined as:

$$\sigma = \langle x_0, \dots, x_m \rangle \in Rips(X, t) \iff f([x_0, \dots, x_m]) \leq t.$$

Homology groups of simplicial complexes provide a formal interpretation of what an n -dimensional “hole” is. Intuitively, a 0-dimensional hole is a connected component, a 1-dimensional hole is a loop, a 2-dimensional hole is a cavity, and so on. Given a simplicial complex K , an m -chain c is a formal sum of m -simplices of K . That is, $c = \sum_{i=1}^k a_i \sigma_i$ where, for $1 \leq i \leq k$, σ_i is an m -simplex of K and a_i is a coefficient in an unital ring R . To relate the m -chains of a given simplicial complex K with its m -dimensional holes, we need the boundary operator ∂_m : If $\langle x_0, \dots, x_m \rangle$ is an m -simplex of K then,

$$\partial_m(\langle x_0, \dots, x_m \rangle) = \sum_{i=0}^m (-1)^i \langle x_0, \dots, x_{i-1}, x_{i+1}, \dots, x_m \rangle.$$

We can extend this definition to any m -chain by linearity. Notice that $\partial_{m-1} \circ \partial_m = 0$ or, in other words, the boundary of a boundary is null. The m -dimensional holes of K are detected from m -chains whose boundary is zero without being “boundaries” themselves. More concretely, the m -dimensional homology group of K is defined as the quotient group

$$H_m(K) = \frac{\text{Ker } \partial_m}{\text{Im } \partial_{m+1}},$$

and its m -dimensional Betti number as $\beta_m = \text{rank } H_m(K)$. Intuitively, β_0 counts the number of independent connected components of K , β_1 the number of independent loops, and so on.

When computed over a field, the homology groups is actually a vector space. This fact allow us to use persistent homology to study filtrations.

Definition 2.4 (persistent homology). Let $\mathcal{F} = (K_t)_{t \in \mathbb{R}}$ be a filtration. Suppose the ground ring R is a field and, therefore, for each $t \in \mathbb{R}$ and $m \in \mathbb{Z}$, the m -dimensional homology group $H_m(K_t)$ is a vector space. For every $a < b$ and m , consider the linear maps $v_m^{a,b} : H_m(K_a) \rightarrow H_m(K_b)$ induced by the inclusion $K_a \hookrightarrow K_b$. The m -th *persistent homology groups* are the images of the linear maps $v_m^{a,b}$, denoted by $\text{Im } v_m^{a,b}$. The set $\{\text{Im } v_m^{a,b}\}_{a < b}$ is called the m -th *persistent homology* of the filtration \mathcal{F} and is denoted by \mathcal{H}_m .

We assume that the rank of $H_m(K_t)$ is finite for all $t \in \mathbb{R}$ and $m \in \mathbb{Z}$. In this case, persistent homology can be compactly represented via persistence barcodes (or diagrams).

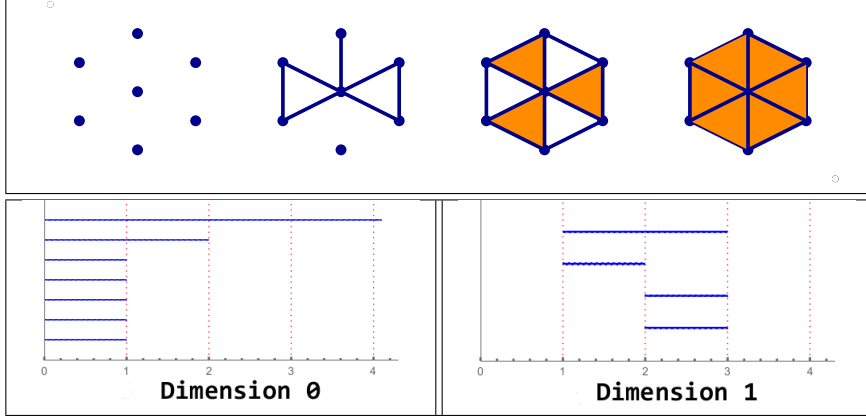


Figure 2: Top: example of a filtration \mathcal{F} . Bottom: 0-th and 1-st persistence barcodes of \mathcal{F} .

Definition 2.5 (persistence barcodes). Let \mathcal{H}_m be the m -th persistent homology of a filtration \mathcal{F} . For $a < b$ and $m \in \mathbb{Z}$, define $\mu_m^{a,b} = (\text{rank}(\text{Im } v_m^{a,b-1}) - \text{rank}(\text{Im } v_m^{a,b})) - (\text{rank}(\text{Im } v_m^{a-1,b-1}) - \text{rank}(\text{Im } v_m^{a-1,b}))$ that can be interpreted as the number of m -dimensional homology classes which are “born” at time a and “die” at time b . Then, \mathcal{H}_m can be represented by the multiset⁴ of intervals $\{[x_i, y_i]\}_{1 \leq i \leq n}$, called the m -th *persistence barcode* or *diagram* of \mathcal{H}_m , where each interval $[x_i, y_i)$ appears $\mu_m^{x_i, y_i}$ times.

In this paper, we assume barcodes have a finite number of elements, find an example in Figure 2. We introduce now the notation used along the paper.

Notation 2.6. Let \mathcal{B} denote the set of persistence barcodes. Given a persistence barcode $A \in \mathcal{B}$, its n_a intervals will be denoted by $[x_i^a, y_i^a)$ for $1 \leq i \leq n_a$. Besides, the length of $[x_i^a, y_i^a)$ will be denoted by ℓ_i^a , that is, $\ell_i^a = y_i^a - x_i^a$. Finally, L_a will denote the sum $\sum_{i=1}^{n_a} \ell_i^a$. Moreover, given two persistence barcodes A and B , denote $\max\{n_a, n_b\}$ by n_{max} and $\max\{L_a, L_b\}$ by L_{max} .

Let us define the following subsets of \mathcal{B} .

Definition 2.7. The set of finite persistence barcodes is defined as:

$$\mathcal{B}_F = \{A \in \mathcal{B} \text{ such that } y_i^a < \infty \text{ for all } [x_i^a, y_i^a) \in A\}.$$

The set of persistence barcodes whose intervals all start at 0 is denoted as \mathcal{B}_0 , that is:

$$\mathcal{B}_0 = \{A \in \mathcal{B} \text{ such that } x_i^a = 0 \text{ for all } [x_i^a, y_i^a) \in A\}$$

And, finally, the set of normalized persistence barcodes is defined as:

$$\mathcal{B}_N = \left\{A \in \mathcal{B} \text{ such that } \sum_{i=1}^{n_a} \ell_i^a = 1\right\}.$$

In the sequel, we will assume that $n_a > 1$ for all $A \in \mathcal{B}_F$ to avoid degenerate cases. There is a correspondence between persistence barcodes in \mathcal{B}_F and persistence barcodes in $\mathcal{B}_0 \cap \mathcal{B}_N$.

Definition 2.8. Let $\psi : \mathcal{B}_F \rightarrow \mathcal{B}_0 \cap \mathcal{B}_N$ be the projection defined as the composition: $\psi = \phi \circ \pi$ where ϕ and π are defined as follows (see Figure 3):

$$\begin{aligned} \phi : \mathcal{B}_F &\rightarrow \mathcal{B}_N \text{ where } A = \{[x_i^a, y_i^a)\}_{1 \leq i \leq n_a} \mapsto \phi(A) = \left\{ \left[\frac{x_i^a}{L_a}, \frac{y_i^a}{L_a} \right) \right\}_{1 \leq i \leq n_a} \\ \pi : \mathcal{B}_F &\rightarrow \mathcal{B}_0 \text{ where } A = \{[x_i^a, y_i^a)\}_{1 \leq i \leq n_a} \mapsto \pi(A) = \{[0, \ell_i^a)\}_{1 \leq i \leq n_a} \end{aligned}$$

The following metrics can be defined on \mathcal{B} .

⁴A multiset is a set whose elements can be repeated

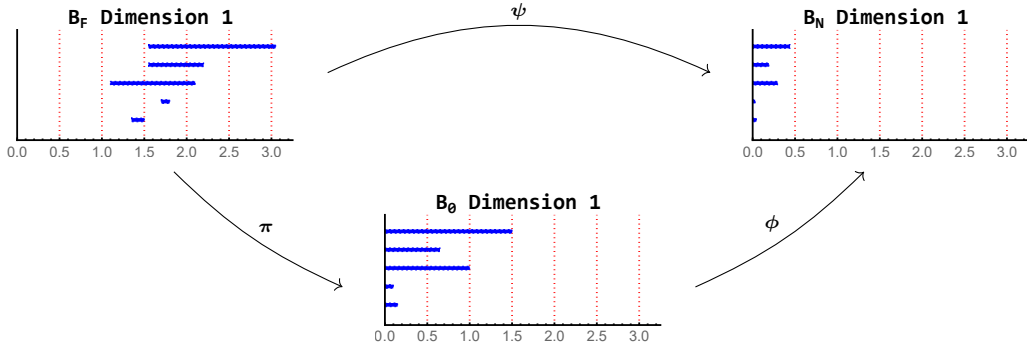


Figure 3: Example of projections π , ϕ and ψ .

Definition 2.9 (Wasserstein and bottleneck distances). Let $A, B \in \mathcal{B}$ and $1 \leq p < \infty$. Define the p -th Wasserstein distance as

$$d_p(A, B) = \left(\min_{\gamma} \sum_{i=1}^{n_{\gamma}} \max \{ |x_i^a - x_{\gamma(i)}^b|^p, |y_i^a - y_{\gamma(i)}^b|^p \} \right)^{\frac{1}{p}}$$

where γ is any bijection between the multisets $A = \{[x_i^a, y_i^a]\}_{1 \leq i \leq n_a}$ and $B = \{[x_i^b, y_i^b]\}_{1 \leq i \leq n_b}$ (including, if necessary, intervals $[t, t]$ of zero length) and n_{γ} is the cardinality⁵ of γ .

The limit case $p = \infty$ is called the *bottleneck distance* and is defined by

$$d_{\infty}(A, B) = \min_{\gamma} \max_i \max \{ |x_i^a - x_{\gamma(i)}^b|, |y_i^a - y_{\gamma(i)}^b| \}.$$

Observe that $n_{\max} \leq n_{\gamma} \leq n_a + n_b$. Besides, in case y_i^a or $y_{\gamma(i)}^b$ is ∞ then $|y_i^a - y_{\gamma(i)}^b|$ is set to ∞ . In case both y_i^a and $y_{\gamma(i)}^b$ are ∞ then $|y_i^a - y_{\gamma(i)}^b|$ is set to 0. Notice also that we have replaced the inf and sup terms of the original definition of Wasserstein and bottleneck distance [7, p. 180-183] by min and max terms because, in this paper, persistence barcodes have always a finite number of intervals.

We finish this section with some well-known persistent homology stability results, supporting the idea that an algorithm designed using persistent homology tools will produce “similar” outputs for “similar” inputs.

Theorem 2.10 ([28]). *Let $f, g : X \rightarrow \mathbb{R}$ be two tame⁶ Lipschitz functions on a metric space X whose triangulations grow polynomially with constant exponent $j \geq 1$. Then, there are constants $c \geq 1$ and $k \geq j$ such that the p -th Wasserstein distance between their corresponding persistence barcodes, denoted by A and B , satisfies:*

$$d_p(A, B) \leq c \|f - g\|_{\infty}^{1 - \frac{k}{p}} \quad \text{for every } p \geq k.$$

When $p = \infty$, the constant c is no longer necessary, obtaining the following most commonly used simplified version.

Corollary 2.11 ([7, p. 183]). *Let K be a simplicial complex and $f, g : K \rightarrow \mathbb{R}$ be two monotonic functions. If A and B denote the corresponding persistence barcodes obtained from f and g , then*

$$d_{\infty}(A, B) \leq \|f - g\|_{\infty}.$$

Finally, as a consequence of Theorem 2.10, we can assert the following.

Theorem 2.12 ([29]). *Consider two finite metric spaces (X, d_X) , (Y, d_Y) . Let A, B be the two persistence barcodes obtained, respectively, from $\text{Rips}(X, t)|_{t \in \mathbb{R}}$ and $\text{Rips}(Y, t)|_{t \in \mathbb{R}}$. Then,*

$$d_{\infty}(A, B) \leq d_{GH}(X, Y)$$

⁵Since γ is a bijection, cardinality of γ refers to the number of elements of the domain of γ which coincides with the number of elements of the image of γ .

⁶The function f is *tame* if there is a finite number of different elements in the set $\{H_m(f^{-1}(-\infty, a])\}_a$ and such set consists of homology groups whose ranks are finite.

where d_{GH} denotes the Gromov-Hausdorff (GH) distance⁷.

Looking at these results, we can conclude that stability results are simpler when using the bottleneck distance than when using the Wasserstein distance.

3 Stability of persistent entropy

This section aims to show under which conditions persistent entropy is stable, which means that it is uniformly continuous or, more informally, there is a bound that “controls” the perturbation produced by noise in the input data. In the first subsection, we recall the definition of persistent entropy. Later, we provide several lemmas that will be needed to prove the stability of persistent entropy for finite persistence barcodes. Lastly, we will see how we can project persistence barcodes with infinite length intervals to finite persistence barcodes in a stable way. These projections will allow to provide general stability results for persistent entropy.

3.1 Persistent entropy

So far, we have seen how persistent homology can be represented using persistence barcodes in a stable way. Nevertheless, sometimes, we might prefer to use only a number to summarize persistent homology (such as persistent entropy), even if we are losing information by doing so.

Definition 3.1 (persistent entropy [12, 11]). The *persistent entropy* $E(A)$ of a persistence barcode $A = \{[x_i^a, y_i^a]\}_{1 \leq i \leq n_a}$ in \mathcal{B}_F is defined as:

$$E(A) = - \sum_{i=1}^{n_a} \frac{\ell_i^a}{L_a} \log \left(\frac{\ell_i^a}{L_a} \right).$$

For simplicity of notation, \log will refer to the log-base-2 function. Observe that, to compute persistent entropy, we only have to consider the length ℓ_i^a of each interval $[x_i^a, y_i^a]$. The following immediate result holds.

Remark 3.2. If $A \in \mathcal{B}_F$ then $E(\psi(A)) = E(A)$.

Let us see now a naive example of application of persistent entropy.

Example 3.3. Suppose we have 20 point clouds: 10 point clouds following a normal distribution and 10 point clouds following a uniform distribution (see Figure 4). Note that since the sample is small, we should not perform a multivariate statistical test, so the idea is to perform univariate statistical tests using persistent entropy. Let us compute the 1-st persistent homology using the Vietoris-Rips filtration. Observe that the computed persistence barcodes will never have infinite length intervals since Vietoris-Rips complexes are always contractible from a (large enough) value. Now, let us compute the persistent entropy of each persistence barcode to obtain a number for each of the point clouds. Let us set $\alpha = 0.05$ and perform the Mann–Whitney U test⁸. We obtain a p -value of $p = 0.046$ for this experiment so $p < \alpha$ and we can conclude that there are significant differences between the point clouds.

Note that, in the definition of persistent entropy, we assume that there are no infinite length intervals in the persistence barcode. We will study in Subsection 3.4 how to proceed when infinite length intervals appear.

3.2 Preliminary lemmas

In this subsection, we will provide several results useful to prove the main results in this paper that will be given in Subsection 3.3.

Let us recall a well-known result regarding p -norms.

⁷The Gromov-Hausdorff distance between X and Y is $\inf_{\gamma_X, \gamma_Y} d_H^Z(\gamma_X(X), \gamma_Y(Y))$ where $d_H^Z(\gamma_X(X), \gamma_Y(Y))$ is the Hausdorff distance between $\gamma_X(X)$ and $\gamma_Y(Y)$ and γ_X, γ_Y range over all the isometric embeddings of X, Y into some same metric space (Z, d_Z) .

⁸See [30] for a simple introduction to statistical tests.

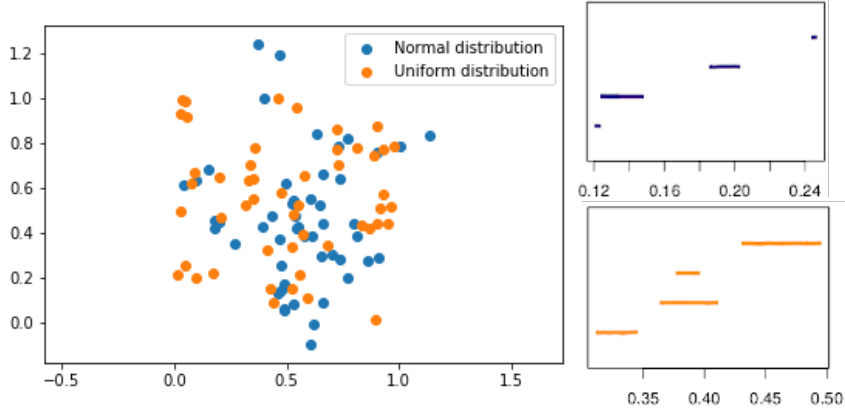


Figure 4: Left: in blue, a point cloud X following a normal distribution; in orange, a point cloud Y following a uniform distribution. Right: 1-th persistence barcode of the Vietoris-Rips filtration associated to X (top) and to Y (bottom).

Remark 3.4. Let $z \in \mathbb{R}^n$ and $p, q \in \mathbb{R}$. Let $\|z\|_p = (\sum_{i=1}^n |z_i|^p)^{\frac{1}{p}}$ and $\|z\|_\infty = \max_i \{|z_i|\}$. If $1 \leq q < p \leq \infty$ then $\|z\|_p \leq \|z\|_q \leq n^{\frac{1}{q} - \frac{1}{p}} \|z\|_p$.

The following result extends Remark 3.4 to the Wasserstein distance.

Lemma 3.5. Let d_p be the p -th Wasserstein distance for persistence barcodes. If $A, B \in \mathcal{B}_F$ and $1 \leq q < p \leq \infty$ then

$$d_p(A, B) \leq d_q(A, B) \leq (n_p)^{\frac{1}{q} - \frac{1}{p}} d_p(A, B).$$

Proof. For $r = p, q$, let γ_r denote a bijection where $d_r(A, B)$ is reached, that is,

$$d_r(A, B) = \left(\sum_{i=1}^{n_r} \max \{|x_i^a - x_{\gamma_r(i)}^b|^r, |y_i^a - y_{\gamma_r(i)}^b|^r\} \right)^{1/r} = \left(\sum_{i=1}^{n_r} (w_{r,i})^r \right)^{1/r}$$

where n_r is the cardinality of γ_r and $w_{r,i} = \max \{|x_i^a - x_{\gamma_r(i)}^b|, |y_i^a - y_{\gamma_r(i)}^b|\}$. Observe that, by definition of d_q and applying Remark 3.4, we have

$$d_q(A, B) \leq \left(\sum_{i=1}^{n_p} (w_{p,i})^q \right)^{\frac{1}{q}} \leq (n_p)^{\frac{1}{q} - \frac{1}{p}} \left(\sum_{i=1}^{n_p} (w_{p,i})^p \right)^{\frac{1}{p}}. \quad (1)$$

Therefore, $d_q(A, B) \leq (n_p)^{\frac{1}{q} - \frac{1}{p}} d_p(A, B)$. Besides, by definition of d_p and again by Remark 3.4,

$$d_p(A, B) \leq \left(\sum_{i=1}^{n_q} (w_{q,i})^p \right)^{\frac{1}{p}} \leq \left(\sum_{i=1}^{n_q} (w_{q,i})^q \right)^{\frac{1}{q}} = d_q(A, B)$$

concluding that $d_p(A, B) \leq d_q(A, B)$. \square

The result below states that when we translate the intervals of given persistence barcodes A and B to the origin by projection π , the distance between them can be doubled.

Lemma 3.6. If $A, B \in \mathcal{B}_F$ then

$$d_p(\pi(A), \pi(B)) \leq 2 d_p(A, B).$$

Proof. Let γ_p be a bijection where $d_p(A, B)$ is reached. Let n_p denote the cardinality of γ_p . Since

$\pi(A) = \{[0, \ell_i^a]\}_{1 \leq i \leq n_a}$ and $\pi(B) = \{[0, \ell_i^b]\}_{1 \leq i \leq n_b}$ then we have:

$$\begin{aligned} (d_p(\pi(A), \pi(B)))^p &= \min_{\gamma} \sum_{i=1}^{n_{\gamma}} \max \{0, |\ell_i^a - \ell_{\gamma(i)}^b|^p\} = \min_{\gamma} \sum_{i=1}^{n_{\gamma}} |\ell_i^a - \ell_{\gamma(i)}^b|^p \\ &\leq \sum_{i=1}^{n_p} |\ell_i^a - \ell_{\gamma_p(i)}^b|^p \leq \sum_{i=1}^{n_p} \left(|x_i^a - x_{\gamma_p(i)}^b| + |y_i^a - y_{\gamma_p(i)}^b| \right)^p \\ &\leq \sum_{i=1}^{n_p} \left(2 \max \{ |x_i^a - x_{\gamma_p(i)}^b|, |y_i^a - y_{\gamma_p(i)}^b| \} \right)^p = 2^p (d_p(A, B))^p. \end{aligned}$$

□

To establish what we consider “big” or “small” error, we need to normalize the distances between persistence barcodes in some way.

Definition 3.7 (relative error). Let $A, B \in \mathcal{B}_F$ and $1 \leq p \leq \infty$. The *relative error* $r_p(A, B)$ is defined as:

$$r_p(A, B) = \frac{2(n_p)^{1-\frac{1}{p}}}{L_{max}} d_p(A, B).$$

Observe that, according to Lemma 3.6, it is satisfied that

$$d_p(\pi(A), \pi(B)) \leq \frac{L_{max}}{(n_p)^{1-\frac{1}{p}}} r_p(A, B).$$

The next lemma is a technical result that we will use later.

Lemma 3.8. *Let γ be a bijection between the multisets $A, B \in \mathcal{B}_F$. Let n_{γ} be the cardinality of γ . Then for all i , $1 \leq i \leq n_{\gamma}$, we have:*

$$\left| \frac{\ell_i^a}{L_a} - \frac{\ell_{\gamma(i)}^b}{L_b} \right| \leq \frac{|\ell_i^a - \ell_{\gamma(i)}^b|}{L_{max}} + \frac{\ell_{\gamma(i)}^b d_1(\pi(A), \pi(B))}{L_a L_b}.$$

Proof. Without loss of generality, suppose $L_{max} = L_a$. Since

$$\left| \frac{\ell_i^a}{L_a} - \frac{\ell_{\gamma(i)}^b}{L_b} \right| = \left| \frac{\ell_i^a L_b - \ell_{\gamma(i)}^b L_a}{L_a L_b} \right| \quad (2)$$

we consider two cases: $\ell_i^a L_b \geq \ell_{\gamma(i)}^b L_a$ and $\ell_i^a L_b \leq \ell_{\gamma(i)}^b L_a$. In the first case:

$$(2) = \frac{\ell_i^a L_b - \ell_{\gamma(i)}^b L_a}{L_a L_b} \leq \frac{\ell_i^a L_b - \ell_{\gamma(i)}^b L_b}{L_a L_b} = \frac{\ell_i^a - \ell_{\gamma(i)}^b}{L_a}.$$

For the second case (i.e., when $\ell_i^a L_b \leq \ell_{\gamma(i)}^b L_a$), use that $L_a \leq L_b + d_1(\pi(A), \pi(B))$ to obtain:

$$\begin{aligned} (2) &= \frac{\ell_{\gamma(i)}^b L_a - \ell_i^a L_b}{L_a L_b} \leq \frac{\ell_{\gamma(i)}^b (L_b + d_1(\pi(A), \pi(B))) - \ell_i^a L_b}{L_a L_b} \\ &= \frac{\ell_{\gamma(i)}^b - \ell_i^a}{L_a} + \frac{\ell_{\gamma(i)}^b d_1(\pi(A), \pi(B))}{L_a L_b}. \end{aligned}$$

□

Let us now see how the projection ψ affects the relationship between the relative error r_p and the distance d_1 .

Lemma 3.9. *If $A, B \in \mathcal{B}_F$ and $1 \leq p \leq \infty$ then*

$$d_1(\psi(A), \psi(B)) \leq 2 r_p(A, B).$$

Proof. Recall that if $A = \{ [x_i^a, y_i^a] \}_{1 \leq i \leq n_a}$ and $B = \{ [x_i^b, y_i^b] \}_{1 \leq i \leq n_b}$ then we have:

$$\begin{aligned} \pi(A) &= \{ [0, \ell_i^a] \}_{1 \leq i \leq n_a} \quad \text{and} \quad \pi(B) = \{ [0, \ell_i^b] \}_{1 \leq i \leq n_b}, \\ \psi(A) &= \left\{ \left[0, \frac{\ell_i^a}{L_a} \right] \right\}_{1 \leq i \leq n_a} \quad \text{and} \quad \psi(B) = \left\{ \left[0, \frac{\ell_i^b}{L_b} \right] \right\}_{1 \leq i \leq n_b}. \end{aligned}$$

Let $\gamma_{\pi,1}$ be a bijection where $d_1(\pi(A), \pi(B))$ is reached, that is:

$$d_1(\pi(A), \pi(B)) = \sum_{i=1}^{n_{\pi,1}} |\ell_i^a - \ell_{\gamma_{\pi,1}(i)}^b|$$

where $n_{\pi,1}$ is the cardinality of $\gamma_{\pi,1}$. Notice that ℓ_i^a or $\ell_{\gamma_{\pi,1}(i)}^b$ might be 0 for some i if intervals of zero length were needed for creating bijection $\gamma_{\pi,1}$. We can assume without loss of generality that $L_{\max} = L_a$. Now by Lemma 3.8 we have:

$$\begin{aligned} d_1(\psi(A), \psi(B)) &\leq \sum_{i=1}^{n_{\pi,1}} \left| \frac{\ell_i^a}{L_a} - \frac{\ell_{\gamma_{\pi,1}(i)}^b}{L_b} \right| \\ &\leq \sum_{i=1}^{n_{\pi,1}} \left(\frac{|\ell_i^a - \ell_{\gamma_{\pi,1}(i)}^b|}{L_a} + \frac{\ell_{\gamma_{\pi,1}(i)}^b d_1(\pi(A), \pi(B))}{L_a L_b} \right) \\ &= \frac{d_1(\pi(A), \pi(B))}{L_a} + \frac{L_b d_1(\pi(A), \pi(B))}{L_a L_b} = \frac{2d_1(\pi(A), \pi(B))}{L_a}. \end{aligned}$$

Applying Lemma 3.6 we have that $\frac{2d_1(\pi(A), \pi(B))}{L_a} \leq \frac{4d_1(A, B)}{L_a}$.

By Lemma 3.5, we get that $\frac{4d_1(A, B)}{L_a} \leq \frac{4(n_p)^{1-\frac{1}{p}} d_p(A, B)}{L_a}$.

Finally, since we assumed that $L_a = L_{\max}$ then $\frac{4(n_p)^{1-\frac{1}{p}} d_p(A, B)}{L_a} = 2r_p(A, B)$. \square

3.3 Stability results for \mathcal{B}_F

Two important results about the stability of persistent homology were recalled in Section 2 (Theorem 2.10 and Theorem 2.12). These results guarantee that if two filter functions (or two metric spaces) are “similar”, then their corresponding persistence barcodes will be “similar” as well. Besides, there also exist stability results for Shannon entropy defined on probability distributions. To combine these results to prove stability of persistent entropy we need to adapt the last ones to the metric space of persistence barcodes.

First of all, recall that the continuity of persistent entropy with respect to the bottleneck distance is proven in [18]. The following proposition generalizes that result to the Wasserstein distance.

Proposition 3.10. *Let $A, B \in \mathcal{B}_F$ and let d_p be the p -th Wasserstein distance with $1 \leq p \leq \infty$. If we fix a maximum number of intervals and a minimum sum of the lengths of the intervals in a persistence barcode, then the persistent entropy E is continuous on (\mathcal{B}_F, d_p) :*

$$\forall \varepsilon \exists \delta \text{ such that } d_p(A, B) \leq \delta \Rightarrow |E(A) - E(B)| \leq \varepsilon.$$

Proof. We have that $d_\infty(A, B) \leq d_p(A, B)$ by Lemma 3.5. Since $d_p(A, B) \leq \delta$ then $d_\infty(A, B) \leq \delta$ and by [18, Proposition 1]

$$d_\infty(A, B) \leq \delta \Rightarrow |E(A) - E(B)| \leq \varepsilon,$$

concluding the proof. \square

The stability of Shannon entropy has been previously studied by Lesche in [31] for the 1-norm due to its importance in physics. That bound can be slightly improved as shown in [32].

Theorem 3.11 ([32, p. 664]). *Let P and Q be two finite probability distributions (seen as vectors in \mathbb{R}^u), and let $E_S(P)$ and $E_S(Q)$ be, respectively, their Shannon entropy. If $\|P - Q\|_1 \leq \frac{1}{2}$ then*

$$|E_S(P) - E_S(Q)| \leq \|P - Q\|_1 (\log(u) - \log(\|P - Q\|_1)).$$

Notice that the restriction $\|P - Q\|_1 \leq \frac{1}{2}$ is reasonable because $\|P - Q\|_1$ is at most 2.

Now, let us introduce one of the main result of this paper. We can observe that since the space $\mathcal{B}_0 \cap \mathcal{B}_N$ can be interpreted as finite probability distributions, we can first project the persistence barcodes of \mathcal{B}_F onto $\mathcal{B}_0 \cap \mathcal{B}_N$ and then apply the previous theorem to obtain the desired stability result.

Theorem 3.12 (stability of persistent entropy). *Let $A, B \in \mathcal{B}_F$. Let us assume that $r_p(A, B) \leq \frac{1}{4}$. Then:*

$$|E(A) - E(B)| \leq 2r_p(A, B) (\log(n_a + n_b) - \log(2r_p(A, B))).$$

Proof. First, by Remark 3.2, we have that

$$|E(A) - E(B)| = |E(\psi(A)) - E(\psi(B))|. \quad (3)$$

Now, let $\gamma_{\psi,1}$ be a bijection where $d_1(\psi(A), \psi(B))$ is reached, that is,

$$d_1(\psi(A), \psi(B)) = \sum_{i=1}^{n_{\psi,1}} \left| \frac{\ell_i^a}{L_a} - \frac{\ell_{\gamma_{\psi,1}(i)}^b}{L_b} \right|$$

where $n_{\psi,1}$ is the cardinality of $\gamma_{\psi,1}$. Let P be the vector $\left(\frac{\ell_1^a}{L_a}, \dots, \frac{\ell_{n_{\psi,1}}^a}{L_a} \right)$ and Q the vector $\left(\frac{\ell_{\gamma_{\psi,1}(1)}^b}{L_b}, \dots, \frac{\ell_{\gamma_{\psi,1}(n_{\psi,1})}^b}{L_b} \right)$. Then, $\|P - Q\|_1 = d_1(\psi(A), \psi(B))$ and by Lemma 3.9,

$$\|P - Q\|_1 = d_1(\psi(A), \psi(B)) \leq 2r_p(A, B).$$

Now, since $r_p(A, B) \leq \frac{1}{4}$ then $\|P - Q\|_1 \leq \frac{1}{2}$. By Theorem 3.11 we have that

$$(3) \leq d_1(\psi(A), \psi(B)) (\log(n_{\psi,1}) - \log d_1(\psi(A), \psi(B))) \quad (4)$$

Now, since $x(\log(n_{\psi,1}) - \log(x))$ is increasing as long as $x \leq \frac{n_{\psi,1}}{e}$ and $d_1(\psi(A), \psi(B)) \leq 2r_p(A, B) \leq \frac{1}{2} \leq \frac{n_{\psi,1}}{e}$ since $n_{\psi,1} \geq 2$ by assumption⁹, then

$$(4) \leq 2r_p(A, B) (\log(n_{\psi,1}) - \log(2r_p(A, B))) \quad (5)$$

Finally,

$$(5) \leq 2r_p(A, B) (\log(n_a + n_b) - \log(2r_p(A, B)))$$

since $n_{\psi,1} \leq n_a + n_b$. \square

Although the bound of $|E(A) - E(B)|$ can tend to ∞ for an arbitrary large n for $n = n_a + n_b$, the relative value $\frac{|E(A) - E(B)|}{\log(n)}$ is bounded when n tends to ∞ since $r_p(A, B) \leq \frac{1}{4}$. In other words,

$$\lim_{n \rightarrow \infty} \sup_{\mathcal{B}_F} \left(\frac{|E(A) - E(B)|}{\log(n)} \right) = 2r_p(A, B).$$

Table 1 shows some numerical examples regarding such relative value.

3.4 Persistence barcodes with infinite length intervals

In order to extend the definition of persistent entropy to persistence barcodes with infinite length intervals, it is common to define a projection from \mathcal{B} to \mathcal{B}_F that transforms infinite length intervals into finite length intervals. There are many ways to do this and depending on choice, persistent entropy may no longer be stable or scale-invariant. In this section, we explain some projections and their properties.

We start with a simple example. To avoid calculations involving the infinite value when computing persistent homology, usually, an upper bound is fixed and considered to be the infinite value. Then, if we want to compute persistent entropy, the first idea could be just to assign this upper bound to each of the infinite values that appear in the infinite length intervals.

⁹See the comment after Notation 2.6.

Table 1: Bounds $\frac{2r_\infty(A,B)(\log(n)-\log(2r_\infty(A,B)))}{\log(n)}$ of relative values $\frac{|E(A)-E(B)|}{\log(n)}$ for different values of n (columns) and relative errors $r_\infty(A, B)$ (rows).

n	$r_\infty(A, B)$			
	0.1	0.05	0.025	0.01
10	0.339794	0.2	0.115051	0.0539794
510	0.251631	0.136933	0.0740258	0.0325498
1010	0.246531	0.133285	0.0716526	0.0313102
1510	0.243975	0.131457	0.070463	0.0306888
2010	0.242321	0.130274	0.0696935	0.0302868
2510	0.24112	0.129415	0.0691346	0.0299949
3010	0.240187	0.128747	0.0687007	0.0297682
3510	0.239431	0.128206	0.0683486	0.0295843
4010	0.238798	0.127754	0.0680541	0.0294305
4510	0.238256	0.127366	0.067802	0.0292988
5010	0.237784	0.127028	0.0675823	0.029184

Definition 3.13 (projection ξ_c). Let $c \in \mathbb{R}$. Define the projection $\xi_c : \mathcal{B} \rightarrow \mathcal{B}_F$ such that for $A = \{[x_i^a, y_i^a]\} \in \mathcal{B}$,

$$\xi_c(A) = \{[x_i^a, z_i^a]\} \text{ where } z_i^a = c \text{ if } y_i^a = \infty \text{ and } z_i^a = y_i^a \text{ otherwise.}$$

The following result confirms that the projection ξ_c is stable.

Proposition 3.14. *Let $A, B \in \mathcal{B}$. Then, projection ξ_c satisfies that*

$$d_p(\xi_c(A), \xi_c(B)) \leq d_p(A, B).$$

Proof. Let $A = \{[x_i^a, y_i^a]\}$ and $B = \{[x_i^b, y_i^b]\}$. Let γ_p be a bijection where $d_p(A, B)$ is reached. Let n_p denote the cardinality of γ_p . Observe that if $y_i^a < \infty$ and $y_{\gamma_p(i)}^b < \infty$ then $|z_i^a - z_{\gamma_p(i)}^b| = |y_i^a - y_{\gamma_p(i)}^b|$. Nevertheless, if $y_i^a = \infty$ and $y_{\gamma_p(i)}^b < \infty$ (resp. $y_i^a < \infty$ and $y_{\gamma_p(i)}^b = \infty$) then $|z_i^a - z_{\gamma_p(i)}^b| < |y_i^a - y_{\gamma_p(i)}^b| = \infty$. Finally, if $y_i^a = y_{\gamma_p(i)}^b = \infty$ then $|z_i^a - z_{\gamma_p(i)}^b| = |y_i^a - y_{\gamma_p(i)}^b| = 0$. We conclude:

$$\begin{aligned} (d_p(\xi_c(A), \xi_c(B)))^p &= \min_{\gamma} \sum_{i=1}^{n_\gamma} \max\{|x_i^a - x_{\gamma(i)}^b|^p, |z_i^a - z_{\gamma(i)}^b|^p\} \\ &\leq \sum_{i=1}^{n_p} \max\{|x_i^a - x_{\gamma_p(i)}^b|^p, |z_i^a - z_{\gamma_p(i)}^b|^p\} \leq (d_p(A, B))^p. \end{aligned}$$

□

Despite being stable, ξ_c is not scale-invariant. By definition, a projection $f : \mathcal{B} \rightarrow \mathcal{B}_F$ is scale-invariant if $f(\lambda A) = \lambda f(A)$, being λA the scalar multiplication of each of the intervals (notice that $\lambda \cdot \infty = \infty$). We now define the following stable and scale-invariant projections from \mathcal{B} to \mathcal{B}_F .

Definition 3.15 (projections $\mu_\lambda, \nu_{\lambda,p}, \tau_\lambda$). Let $\lambda \geq 0$ and $1 \leq p \leq \infty$. Let $A = \{[x_i^a, y_i^a]\} \in \mathcal{B}$. Then:

- $\mu_\lambda(A) = \{[x_i^a, z_i^a]\}$ where $z_i^a = x_i^a + \lambda \ell_{max}^a$ if $y_i^a = \infty$ and $z_i^a = y_i^a$ otherwise; being ℓ_{max}^a the maximum finite value for $\ell_i^a = y_i^a - x_i^a$.
- $\nu_{\lambda,p}(A) = \{[x_i^a, z_i^a]\}$ where $z_i^a = x_i^a + \lambda L_{a,p}$ if $y_i^a = \infty$ and $z_i^a = y_i^a$ otherwise; being $L_{a,p} = (\sum_{i \in I} (\ell_i^a)^p)^{1/p}$ where $I = \{i : 1 \leq i \leq n_a \text{ and } \ell_i^a < \infty\}$.
- $\tau_\lambda(A) = \{[x_i^a, z_i^a]\}$ where $z_i^a = (1 + \lambda)u_a$ if $y_i^a = \infty$ and $z_i^a = y_i^a$ otherwise; being u_a the maximum finite value for y_i^a .

Notice that $\mu_0 = \nu_{0,p}$ and both are equivalent to remove the infinite length intervals.

Proposition 3.16 (stability of projections $\tau_\lambda, \mu_\lambda, \nu_{\lambda,p}$). *Given two persistence barcodes $A, B \in \mathcal{B}$ with the same number m of infinite length intervals, we have that:*

$$\begin{aligned} d_p(\mu_\lambda(A), \mu_\lambda(B)) &\leq (1 + m2^p\lambda^p)^{1/p} d_p(A, B); \\ d_p(\nu_{\lambda,p}(A), \nu_{\lambda,p}(B)) &\leq (1 + m2^p\lambda^p)^{1/p} d_p(A, B). \end{aligned}$$

If the length of the longest finite interval in A and B are both greater than $2d_\infty(A, B)$, then

$$d_p(\tau_\lambda(A), \tau_\lambda(B)) \leq (1 + m(1 + \lambda)^p)^{1/p} d_p(A, B).$$

Proof. Sort the intervals of A and B such that their first m intervals are the infinite length intervals and for $r = p, \infty$, consider a bijection γ_r where $d_r(A, B)$ is reached. Let n_r denote the cardinality of γ_r . Let f refer to $\tau_\lambda, \mu_\lambda$ or $\nu_{\lambda,p}$. We have:

$$\begin{aligned} (d_p(f(A), f(B)))^p &= \min_\gamma \sum_{i=1}^{n_\gamma} \max \{ |x_i^a - x_{\gamma(i)}^b|^p, |z_i^a - z_{\gamma(i)}^b|^p \} \\ &\leq \sum_{i=1}^{n_p} \max \{ |x_i^a - x_{\gamma_p(i)}^b|^p, |z_i^a - z_{\gamma_p(i)}^b|^p \} \\ &= \sum_{i=1}^m \max \{ |x_i^a - x_{\gamma_p(i)}^b|^p, |z_i^a - z_{\gamma_p(i)}^b|^p \} + \sum_{i=m+1}^{n_p} \max \{ |x_i^a - x_{\gamma_p(i)}^b|^p, |y_i^a - y_{\gamma_p(i)}^b|^p \} \\ &= \sum_{i=1}^m \max \{ |x_i^a - x_{\gamma_p(i)}^b|^p, |z_i^a - z_{\gamma_p(i)}^b|^p \} + (d_p(A, B))^p - \sum_{i=1}^m |x_i^a - x_{\gamma_p(i)}^b|^p \\ &= \sum_{i=1}^m \max \{ 0, |z_i^a - z_{\gamma_p(i)}^b|^p - |x_i^a - x_{\gamma_p(i)}^b|^p \} + (d_p(A, B))^p \\ &= \sum_{i=1}^m (|z_i^a - z_{\gamma_p(i)}^b|^p - |x_i^a - x_{\gamma_p(i)}^b|^p) + (d_p(A, B))^p. \end{aligned}$$

If $f = \mu_\lambda$ then, for all $i, 1 \leq i \leq m$, we have:

$$\begin{aligned} |z_i^a - z_{\gamma_p(i)}^b|^p - |x_i^a - x_{\gamma_p(i)}^b|^p &= |\lambda \ell_{max}^a - x_i^a - \lambda \ell_{max}^b + x_{\gamma_p(i)}^b|^p - |x_i^a - x_{\gamma_p(i)}^b|^p \\ &\leq |x_i^a - x_{\gamma_p(i)}^b|^p + |\lambda \ell_{max}^a - \lambda \ell_{max}^b|^p - |x_i^a - x_{\gamma_p(i)}^b|^p = \lambda^p |\ell_{max}^a - \ell_{max}^b|^p. \end{aligned}$$

Assume, without loss of generality, that $\ell_{max}^a \geq \ell_{max}^b$. Then, the interval with length ℓ_*^b paired to an interval with length ℓ_{max}^a by bijection γ_∞ satisfies, by definition, that $\ell_*^b \leq \ell_{max}^b \leq \ell_{max}^a$ and then

$$|\ell_{max}^a - \ell_{max}^b| \leq |\ell_{max}^a - \ell_*^b| \leq 2d_\infty(A, B),$$

obtaining

$$|z_i^a - z_{\gamma_p(i)}^b|^p - |x_i^a - x_{\gamma_p(i)}^b|^p \leq 2^p \lambda^p (d_\infty(A, B))^p$$

and

$$\begin{aligned} &\sum_{i=1}^m (|z_i^a - z_{\gamma_p(i)}^b|^p - |x_i^a - x_{\gamma_p(i)}^b|^p) + (d_p(A, B))^p \\ &\leq m2^p \lambda^p (d_\infty(A, B))^p + (d_p(A, B))^p \leq (m2^p \lambda^p + 1) (d_p(A, B))^p. \end{aligned}$$

If $f = \nu_{\lambda,p}$ then, for all $i, 1 \leq i \leq m$, we have:

$$\begin{aligned} |z_i^a - z_{\gamma_p(i)}^b|^p - |x_i^a - x_{\gamma_p(i)}^b|^p &= \left| x_i^a + \lambda L_{a,p} - x_{\gamma_p(i)}^b - \lambda L_{b,p} \right|^p - |x_i^a - x_{\gamma_p(i)}^b|^p \\ &\leq |\lambda L_{a,p} - \lambda L_{b,p}|^p + |x_i^a - x_{\gamma_p(i)}^b|^p - |x_i^a - x_{\gamma_p(i)}^b|^p = \lambda^p |L_{a,p} - L_{b,p}|^p. \end{aligned}$$

By the reverse triangle inequality:

$$\lambda^p |L_{a,p} - L_{b,p}|^p \leq \lambda^p \sum_{i=m+1}^{n_{\pi,p}} |\ell_i^a - \ell_{\gamma_{\pi,p}(i)}^b|^p \leq \lambda^p (d_p(\pi(A), \pi(B)))^p$$

being $n_{\pi,p}$ the cardinal of a bijection $\gamma_{\pi,p}$ where $d_p(\pi(A), \pi(B))$ is reached. By Lemma 3.6,

$$\lambda^p (d_p(\pi(A), \pi(B)))^p \leq 2^p \lambda^p (d_p(A, B))^p$$

and finally,

$$\sum_{i=1}^m (|z_i^a - z_{\gamma_p(i)}^b|^p - |x_i^a - x_{\gamma_p(i)}^b|^p) + (d_p(A, B))^p \leq (m2^p \lambda^p + 1)(d_p(A, B))^p.$$

If $f = \tau_\lambda$ then

$$\begin{aligned} & \sum_{i=1}^m (|z_i^a - z_{\gamma_p(i)}^b|^p - |x_i^a - x_{\gamma_p(i)}^b|^p) + (d_p(A, B))^p \\ & \leq \sum_{i=1}^m |z_i^a - z_{\gamma_p(i)}^b|^p + (d_p(A, B))^p = (1 + \lambda)^p m |u^a - u^b|^p + (d_p(A, B))^p. \end{aligned}$$

We only have to prove that $|u^a - u^b| \leq d_\infty(A, B)$. By reduction to the absurd, suppose that $u^a - u^b > d_\infty(A, B)$. Without loss of generality, assume $u^a \geq u^b$. Take one interval α in A with endpoint u^a and another one in B with endpoint u^b . Since, by hypothesis, the length of both intervals is greater than $2d_\infty(A, B)$ then we can assume that they are not paired with the diagonal when computing the bottleneck distance. Let $[x^b, y^b]$ be the interval in B paired with α . Then

$$u^a - y^b \leq d_\infty(A, B) < u^a - u^b \Rightarrow u^b < y^b$$

leading to a contradiction. Therefore,

$$\begin{aligned} (1 + \lambda)m |u^a - u^b|^p + (d_p(A, B))^p & \leq (1 + \lambda)^p m (d_\infty(A, B))^p + (d_p(A, B))^p \\ & \leq ((1 + \lambda)^p m + 1) (d_p(A, B))^p. \end{aligned}$$

□

Of course, these projections are just a few of the many possible that can be defined. In the past, since persistent entropy only takes into account the length of the intervals, infinite length intervals were usually replaced by intervals of a fixed finite length. For example, in [14], τ_1 was used plus a constant. With respect to this case, notice that adding a constant in the definition of any of the projections above will produce stable but not scale-invariant projections. In [16], infinite length intervals were ignored using the stable and scale-invariant projection μ_0 obtaining a topological based variable for analyzing cell arrangement.

3.5 Stability results for \mathcal{B}

Let us now introduce the following results on the stability of persistent entropy for the general case. For simplicity, we have removed infinite length intervals using μ_0 for these statements, but we could use any other stable projection to remove such intervals. This way, the formulas that appear in the statements below would change according to the inequalities of Proposition 3.16.

Theorem 3.17. *Let K be a simplicial complex and let $f, g : K \rightarrow \mathbb{R}$ be two monotonic functions. Let $A, B \in \mathcal{B}$ be their corresponding persistence barcodes. If $\|f - g\|_\infty \leq \frac{1}{8} \frac{L_{max}}{n}$ then*

$$|E(\mu_0(A)) - E(\mu_0(B))| \leq \frac{4n \|f - g\|_\infty}{L_{max}} \left(\log(n) - \log \left(\frac{4n \|f - g\|_\infty}{L_{max}} \right) \right).$$

where $n = n_a + n_b$, being n_a (resp. n_b) the number of intervals of $\mu_0(A)$ (resp. $\mu_0(B)$).

Proof. First, using Corollary 2.11, we have that $d_\infty(A, B) \leq \|f - g\|_\infty$. Then,

$$r_\infty(\mu_0(A), \mu_0(B)) = \frac{2d_\infty(A, B)n_\infty}{L_{max}} \leq \frac{2\|f - g\|_\infty n_\infty}{L_{max}} \leq \frac{1}{4}.$$

Therefore, by Theorem 3.12, we have:

$$|E(\mu_0(A)) - E(\mu_0(B))| \leq 2r_\infty(\mu_0(A), \mu_0(B)) (\log(n) - \log(2r_\infty(\mu_0(A), \mu_0(B))))).$$

Since the function $x(\log(n) - \log(x))$ is increasing as long as $x \leq \frac{n}{e}$ and $\frac{1}{2} \leq \frac{n}{e}$ since $n \geq 2$ by assumption, then

$$\begin{aligned} & 2r_\infty(\mu_0(A), \mu_0(B)) (\log(n) - \log(2r_\infty(\mu_0(A), \mu_0(B)))) \\ & \leq \frac{4n\|f - g\|_\infty}{L_{max}} \left(\log(n) - \log\left(\frac{4n\|f - g\|_\infty}{L_{max}}\right) \right). \end{aligned}$$

□

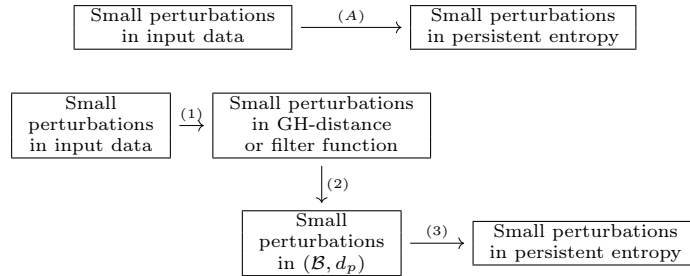
Theorem 3.18. *Let A, B be the persistence barcodes obtained respectively from $Rips(X, t)|_{t \in \mathbb{R}}$ and $Rips(Y, t)|_{t \in \mathbb{R}}$, being (X, d_X) and (Y, d_Y) two finite metric spaces. If $d_{GH}(X, Y) \leq \frac{1}{8} \frac{L_{max}}{n}$ then,*

$$|E(\mu_0(A)) - E(\mu_0(B))| \leq \frac{4nd_{GH}(X, Y)}{L_{max}} \left(\log(n) - \log\left(\frac{4nd_{GH}(X, Y)}{L_{max}}\right) \right).$$

where $n = n_a + n_b$, being n_a (resp. n_b) the number of intervals of $\mu_0(A)$ (resp. $\mu_0(B)$).

Proof. Using Theorem 2.12 we have that $d_\infty(A, B) \leq d_{GH}(X, Y)$. As in the proof of Theorem 3.17 since $d_{GH}(X, Y) \leq \frac{1}{8} \frac{L_{max}}{n}$ and the function $x(\log(n) - \log(x))$ is increasing as long as $x \leq \frac{n}{e}$ then, by Theorem 3.12, we obtain the desired result. □

It seems appropriate now to recapitulate the results of this section before moving on. As shown in the following diagram, at the beginning of the section we wanted to prove implication (A). In order to do it, we separated the problem into three parts ((1), (2) and (3)):



Implication (1) is given by the formalization of the problem and implication (2) is given by Theorem 2.10 and Theorem 2.12 mentioned in the background section. The proof of implication (3) is the main aim of this section (Theorem 3.12). Putting all together we obtain Theorem 3.17 and Theorem 3.18.

4 Entropy-based summary functions

As we have already mentioned, numbers summarizing persistence barcodes (such as persistent entropy) are very useful to perform statistical tests. Nevertheless, if we want to perform a classification task, their discriminatory power might not be enough. One of the possible solutions is to summarize persistence barcodes using functions. Summary functions (such as the already mentioned persistence silhouettes, Euler characteristic curves, topological intensity maps or persistence landscapes) have been used in the past to obtain statistical information from persistence barcodes. For example, a simple but effective way of summarizing a persistence barcode is the *Betti curve* defined as follows: If $A = \{[x_i^a, y_i^a]\} \in \mathcal{B}$ then

$$\beta(A)[t] = \text{cardinality of } \{[x_i^a, y_i^a] : x_i^a \leq t \leq y_i^a\}.$$

That is, $\beta(A)(t)$ is the number of intervals in A which are “alive” at time t .

In this section, we will define a new summary piece-wise constant function (also known as step function). It is similar to the Betti curve but uses persistent entropy instead of Betti numbers. We will prove its stability and show examples where such function measures different features of the persistence barcode than the Betti curve. Besides, and contrary to what happened with persistent entropy, we will see that the normalization of this function is also stable.

4.1 Entropy summary function (ES-function)

We now define a new function that pairs a persistence barcode $A \in \mathcal{B}_F$ with a real-valued piecewise constant function. This new function summarizes information about the number of intervals of a given persistence barcode and their homogeneity and, as we will prove at the end of this subsection, is stable with respect to the bottleneck distance.

Definition 4.1 (ES-function). The entropy summary function (ES-function) of a persistence barcode $A = \{[x_i^a, y_i^a]\}_{1 \leq i \leq n_a}$ in \mathcal{B}_F is the real-valued piecewise linear function:

$$S(A)[t] = - \sum_{i=1}^{n_a} w_i^a(t) \frac{\ell_i^a}{L_a} \log \left(\frac{\ell_i^a}{L_a} \right)$$

where $w_i^a(t) = 1$ if $x_i^a \leq t \leq y_i^a$ and $w_i^a(t) = 0$ otherwise.

In other words, the ES-function pairs a persistence barcode $A = \{[x_i^a, y_i^a]\}$ and an instant t with the partial sum of $E(A)$ corresponding to the intervals $[x_i^a, y_i^a]$ of A that are “alive” at that moment t , that is, $x_i^a \leq t \leq y_i^a$. See Figure 5. Notice that $S(A) : \mathbb{R} \rightarrow \mathbb{R}$ and $S : \mathcal{B}_F \rightarrow \mathcal{C}$, being \mathcal{C} the space of real-valued piece-wise constant functions.

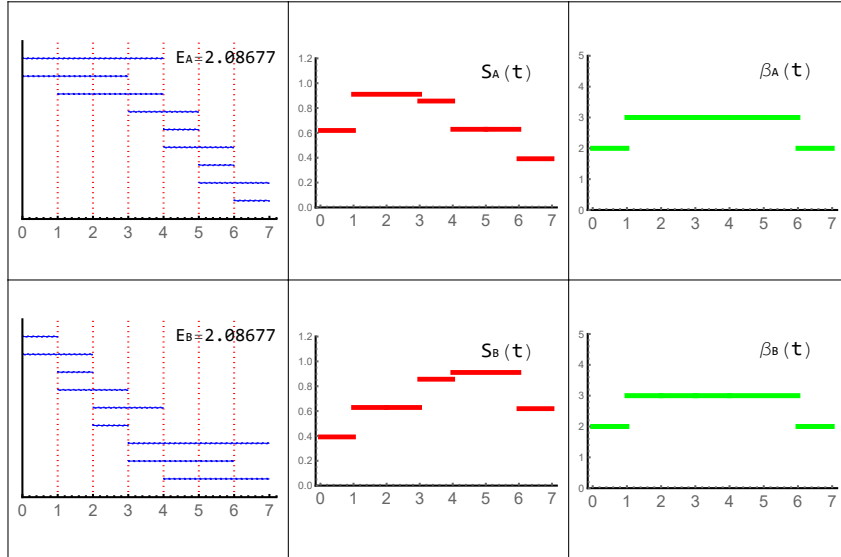


Figure 5: In this example we can see two different persistence barcodes for which their Betti curves and persistent entropy are the same but not their ES-function.

The following result states that the ES-function is stable with respect to the bottleneck distance.

Theorem 4.2 (stability of the ES-function). Let S be the ES-function, d_∞ the bottleneck distance and A, B two persistence barcodes in \mathcal{B}_F . Let n_∞ be the cardinality of a bijection, denoted as γ_∞ , where $d_\infty(A, B)$ is reached. If $r_\infty(A, B) \leq \frac{2}{3e}$ then:

$$\|S(A) - S(B)\|_1 \leq r_\infty(A, B) L_{max} \left(\frac{\log n_{max}}{n_{max}} - \frac{3}{2} \log \left(\frac{3}{2} r_\infty(A, B) \right) \right).$$

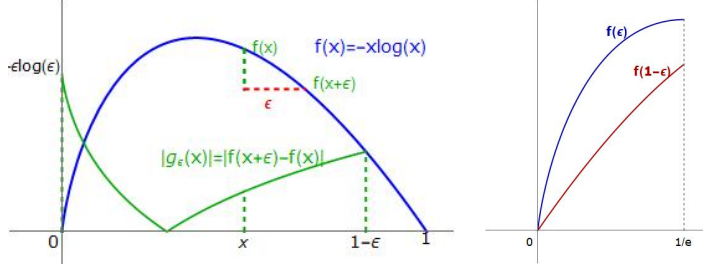


Figure 6: On the left, $|g_\epsilon(x)|$ is pictured in green and $f(x)$ in blue. On the right, observe that $f(\epsilon) > f(1 - \epsilon)$ for $\epsilon \in (0, 1/e)$, so $|g_\epsilon(x)|$ attains the global maximum on $[0, 1 - \epsilon]$ at $x = 0$.

Proof. Denote the expression $\frac{\ell_i^a}{L_a} \log\left(\frac{\ell_i^a}{L_a}\right)$ by s_i^a . Then,

$$\begin{aligned}
\|S(A) - S(B)\|_1 &= \left\| \sum_i^{n_\infty} w_i^a s_i^a - w_{\gamma_\infty(i)}^b s_{\gamma_\infty(i)}^b \right\|_1 \\
&= \left\| \sum_i^{n_\infty} (w_i^a w_{\gamma_\infty(i)}^b + w_i^a (1 - w_{\gamma_\infty(i)}^b)) s_i^a - (w_{\gamma_\infty(i)}^b w_i^a + w_{\gamma_\infty(i)}^b (1 - w_i^a)) s_{\gamma_\infty(i)}^b \right\|_1 \\
&= \left\| \sum_i^{n_\infty} w_i^a w_{\gamma_\infty(i)}^b (s_i^a - s_{\gamma_\infty(i)}^b) + w_i^a (1 - w_{\gamma_\infty(i)}^b) s_i^a - w_{\gamma_\infty(i)}^b (1 - w_i^a) s_{\gamma_\infty(i)}^b \right\|_1 \\
&\leq \sum_i^{n_\infty} \|w_i^a w_{\gamma_\infty(i)}^b\|_1 |s_i^a - s_{\gamma_\infty(i)}^b| + \|w_i^a (1 - w_{\gamma_\infty(i)}^b) s_i^a\|_1 + \|w_{\gamma_\infty(i)}^b (1 - w_i^a) s_{\gamma_\infty(i)}^b\|_1.
\end{aligned}$$

Let us now compute a bound for $\sum_{i=1}^{n_\infty} \|w_i^a w_{\gamma_\infty(i)}^b\|_1 |s_i^a - s_{\gamma_\infty(i)}^b|$. Without loss of generality, assume that $L_a \geq L_b$. Since $\|w_i^a w_{\gamma_\infty(i)}^b\|_1$ represents the length of the intersection of non-null paired intervals, we have that

$$\sum_i^{n_\infty} \|w_i^a w_{\gamma_\infty(i)}^b\|_1 \leq L_a. \quad (6)$$

Let us compute a bound for $|s_i^a - s_{\gamma_\infty(i)}^b|$. Denote the expression $\left| \frac{\ell_i^a}{L_a} - \frac{\ell_{\gamma_\infty(i)}^b}{L_b} \right|$ by ϵ . By Lemma 3.8 and Lemma 3.9, we have that

$$\begin{aligned}
\epsilon &\leq \frac{|\ell_i^a - \ell_{\gamma_\infty(i)}^b|}{L_a} + \frac{\ell_{\gamma_\infty(i)}^b d_1(\pi(A), \pi(B))}{L_a L_b} \\
&\leq \frac{2 \max\{|x_i^a - x_{\gamma_\infty(i)}^b|, |y_i^a - y_{\gamma_\infty(i)}^b|\}}{L_a} + \frac{L_b d_1(\pi(A), \pi(B))}{L_a L_b} \\
&\leq \frac{2d_\infty(A, B)}{L_a} + \frac{2d_1(A, B)}{L_a} \leq \frac{2d_\infty(A, B)}{L_a} + \frac{2n_\infty d_\infty(A, B)}{L_a} \\
&\leq \frac{(2 + 2n_\infty)d_\infty(A, B)}{L_a} \leq \frac{3n_\infty d_\infty(A, B)}{L_a} = \frac{3}{2} r_\infty(A, B). \quad (7)
\end{aligned}$$

By hypothesis, we have that $r_\infty(A, B) \leq \frac{2}{3e}$, so $\frac{3}{2} r_\infty(A, B) \leq \frac{1}{e}$. Then, $\epsilon \leq \frac{1}{e}$. Now, recall that $f(x) = -x \log x$ is continuous and concave in $[0, 1]$ with $f(0) = f(1) = 0$ and consider the function $g_\epsilon(x) = f(x + \epsilon) - f(x)$ defined for any $x \in [0, 1 - \epsilon]$. As f is concave and differentiable in $(0, 1)$, f' is decreasing, g'_ϵ is negative and so g_ϵ is decreasing monotone. Therefore the maximum of its absolute value is attained at one of the extreme points of the interval $[0, 1 - \epsilon]$. Observe that since $\epsilon \leq \frac{1}{e}$, this maximum is reached at $x = 0$ (see Figure 6):

$$\begin{aligned}
|g_\epsilon(x)| &= |f(x + \epsilon) - f(x)| \leq \max\{|f(\epsilon) - f(0)|, |f(1) - f(1 - \epsilon)|\} \\
&= \max\{-\epsilon \log(\epsilon), -(1 - \epsilon) \log(1 - \epsilon)\} = -\epsilon \log(\epsilon). \quad (8)
\end{aligned}$$

Now, using (8), we obtain that:

$$|s_i^a - s_{\gamma_\infty(i)}^b| = \left| \frac{\ell_i^a}{L_a} \log \left(\frac{\ell_i^a}{L_a} \right) - \frac{\ell_{\gamma_\infty(i)}^b}{L_b} \log \left(\frac{\ell_{\gamma_\infty(i)}^b}{L_b} \right) \right| \leq -\epsilon \log(\epsilon). \quad (9)$$

Due to (7) and $f(x) = -x \log x$ being increasing in $[0, \frac{1}{e}]$, we obtain from (9) that:

$$|s_i^a - s_{\gamma_\infty(i)}^b| \leq -\frac{3}{2} r_\infty(A, B) \log \left(\frac{3}{2} r_\infty(A, B) \right). \quad (10)$$

Finally, by (6) and (10), we have:

$$\sum_i^{n_\infty} \|w_i^a w_{\gamma_\infty(i)}^b\|_1 |s_i^a - s_{\gamma_\infty(i)}^b| \leq -\frac{3}{2} L_a r_\infty(A, B) \log \left(\frac{3}{2} r_\infty(A, B) \right). \quad (11)$$

Now, let us compute a bound for

$$\sum_i^{n_\infty} \|w_i^a (1 - w_{\gamma_\infty(i)}^b) s_i^a\|_1 + \|w_{\gamma_\infty(i)}^b (1 - w_i^a) s_{\gamma_\infty(i)}^b\|_1.$$

Consider the function $w_{\gamma_\infty(i)}^b (1 - w_i^a)$. Its integral gives the ‘‘period of time’’ in which the $\gamma_\infty(i)$ -th interval of B , $[x_{\gamma_\infty(i)}^b, y_{\gamma_\infty(i)}^b]$, is ‘‘alive’’ and the i -th interval of A , $[x_i^a, y_i^a]$, is not. This might happen in both the initial and the end of the intervals. Therefore, if $\epsilon_i = \max\{|x_i^a - x_{\gamma_\infty(i)}^b|, |y_i^a - y_{\gamma_\infty(i)}^b|\}$ then:

$$\int_{\mathbb{R}} w_{\gamma_\infty(i)}^b(t) (1 - w_i^a(t)) dt \leq 2\epsilon_i.$$

We also have that, in the case where $\epsilon_i < \int_{\mathbb{R}} w_{\gamma_\infty(i)}^b(t) (1 - w_i^a(t)) dt$, the period of time where the i -th interval of A is alive and the one of B is not, is null. Therefore

$$\epsilon_i < \int_{\mathbb{R}} w_{\gamma_\infty(i)}^b(t) (1 - w_i^a(t)) dt \Rightarrow \int_{\mathbb{R}} w_i^a(t) (1 - w_{\gamma_\infty(i)}^b(t)) dt = 0$$

and vice-versa. Using both previous statements and that $\sum_{i=1}^{n_a} s_i^a = E(A)$ we can deduce:

$$\begin{aligned} & \sum_i^{n_\infty} s_i^a \left\| w_i^a (1 - w_{\gamma_\infty(i)}^b) \right\|_1 + s_{\gamma_\infty(i)}^b \left\| w_{\gamma_\infty(i)}^b (1 - w_i^a) \right\|_1 \\ & \leq \sum_i^{n_\infty} s_i^a \int_{\mathbb{R}} w_i^a (1 - w_{\gamma_\infty(i)}^b) + s_{\gamma_\infty(i)}^b \int_{\mathbb{R}} w_{\gamma_\infty(i)}^b (1 - w_i^a) \\ & \leq \max \left\{ \sum_i^{n_\infty} \epsilon_i (s_i^a + s_{\gamma_\infty(i)}^b), \sum_i^{n_\infty} 2\epsilon_i s_i^a, \sum_i^{n_\infty} 2\epsilon_i s_{\gamma_\infty(i)}^b \right\} \\ & \leq \max \left\{ \max_i \{\epsilon_i\} \left(\sum_i^{n_\infty} s_i^a + \sum_i^{n_\infty} s_{\gamma_\infty(i)}^b \right), 2 \max_i \{\epsilon_i\} \sum_i^{n_\infty} s_i^a, 2 \max_i \{\epsilon_i\} \sum_i^{n_\infty} s_{\gamma_\infty(i)}^b \right\} \\ & = \max \left\{ \max_i \{\epsilon_i\} \left(\sum_i^{n_a} s_i^a + \sum_i^{n_b} s_i^b \right), 2 \max_i \{\epsilon_i\} \sum_i^{n_a} s_i^a, 2 \max_i \{\epsilon_i\} \sum_i^{n_b} s_i^b \right\} \\ & \leq d_\infty(A, B) \max \{E(A) + E(B), 2E(A), 2E(B)\} \leq r_\infty(A, B) \frac{L_a}{n_{\max}} \log(n_{\max}). \end{aligned}$$

From this last equation and (11), we obtain the desired result. \square

Notice that the ES-function is based on persistent entropy whereas the Betti curve consists of counting the number of ‘‘alive’’ intervals. Both functions (the ES-function and the Betti curve) are continuous with respect to the bottleneck distance if the maximum number of intervals is fixed. Nevertheless, the ES-function is expected to perform better than the Betti curve in a noisy context since persistent entropy is stable while counting the number of intervals is not, even if it is continuous.

4.2 Normalized entropy summary function (NES-function)

One of the main aims of persistent homology is to represent the shape of the input data. In some applications, like image analysis or material science (see [33] for a review), it may be important to detect some repetitive pattern independently of the size of the input dataset. A possible tool to do this is a normalized version of the summary function, in order to try to capture the shape of the space and not the size.

Definition 4.3 (NES-function). The normalized entropy summary function (NES-function) of a persistence barcode $A = \{[x_i^a, y_i^a]\}_{1 \leq i \leq n_a}$ in \mathcal{B}_F is defined as:

$$NES(A)[t] = \frac{S(A)[t]}{\|S(A)\|_1}.$$

Like the ES-function, this function is also stable.

Theorem 4.4 (Stability of the NES-function). *Under the same hypothesis as in Theorem 4.2, we have that:*

$$\|NES(A) - NES(B)\|_1 \leq \frac{r_\infty(A, B)L_{max} \left(\frac{\log n_{max}}{n_{max}} - \frac{3}{2} \log \left[\frac{3}{2} r_\infty(A, B) \right] \right)}{\min\{\|S(A)\|_1, \|S(B)\|_1\}}.$$

Proof. First, observe that

$$\begin{aligned} \left\| \frac{S(A)}{\|S(A)\|_1} - \frac{S(B)}{\|S(B)\|_1} \right\|_1 &= \frac{\| \|S(B)\|_1 S(A) - \|S(A)\|_1 S(B) \|_1}{\|S(A)\|_1 \|S(B)\|_1} \\ &\leq \frac{\max\{\|S(A)\|_1 \|S(B)\|_1\} (\|S(A) - S(B)\|_1)}{\|S(A)\|_1 \|S(B)\|_1} = \frac{\|S(A) - S(B)\|_1}{\min\{\|S(A)\|_1, \|S(B)\|_1\}}. \end{aligned}$$

Apply Theorem 4.2 to bound $\|S(A) - S(B)\|_1$ obtaining the desired result. \square

5 Experimentation

Our summary functions have been recently applied to real-world data in [34] and [35]. The authors of these papers explicitly mentioned the stability of these functions, presented here and in the arXiv version [36], to guarantee the robustness of their methods. In [34] an algorithm is developed for segmenting and classifying different types of skin lesions in a given skin image. The database used is the International Skin Imaging Collaboration (ISIC) dataset¹⁰ consisting of 10015 skin lesion images. In the classification part, the authors first computed the persistence diagram for each channel of the image in different color space. Then, topological features including our ES-function (referred as “persistent entropy curves”) and Betti curves were calculated from persistence diagrams obtained previously. Finally, the authors used multi-class support vector machine with a “one-against-one” strategy. The best 3 scores they had on the validation set was 65.6%, 66%, and 67.2% depending on the color space used. Besides, in [35], the authors developed a general framework called “persistence curves” for vectorizing persistence diagrams inspired in our ES-function, referred in [35] as “life entropy”, denoted by le , and used for texture classification on four different texture datasets. They showed that a combination of different flavors of persistence curves (including our ES-function) produces the best result, showing that they are complementary to each other.

This section is devoted to experiments. In Subsection 5.1 we study how the NES-function and similar vectorizations such as the Betti curves and the persistence silhouettes may benefit from each other in machine learning tasks. The dataset considered in our experiment consists of miscellaneous real-world images taken from the USC-SIPI Image Database¹¹. The machine learning method used in our experiment is the random forest technique [37]. Later, in Subsection 5.2, we will also add persistence images to our experiment to see how different vectorization methods perform depending on the nature of the data sets. In particular, we will consider the Flickr Material Database (FMD)¹². The whole experiment has been developed in Python and R. Scripts

¹⁰<https://www.isic-archive.com>

¹¹<http://sipi.usc.edu/database/database.php?volume=misc>

¹²<https://people.csail.mit.edu/ceciu/CVPR2010/FMD/>

and notebooks can be downloaded from here¹³. Libraries used are scikit-TDA¹⁴ (in particular Persim¹⁵ and Ripser¹⁶), scikit-image¹⁷, scikit-learn¹⁸ and R-TDA-package¹⁹.

5.1 USC-SIPI dataset experiment

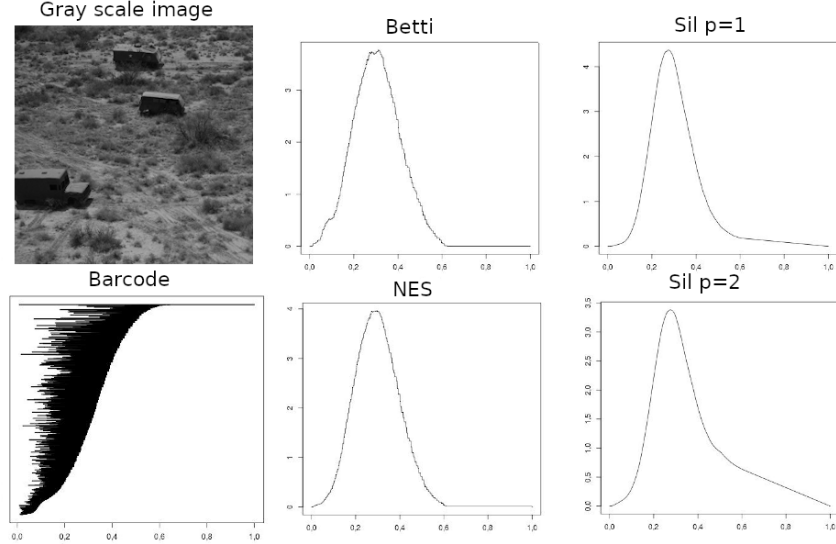


Figure 7: Left: a gray scale image from the USC-SIPI Image Database and its associated 0-th persistence barcode used to compute the summary functions. Center: the Betti curve and the NES-function. Right: The persistence silhouettes for $p = 1$ and $p = 2$. Observe that, in this example, outputs are extremely similar.

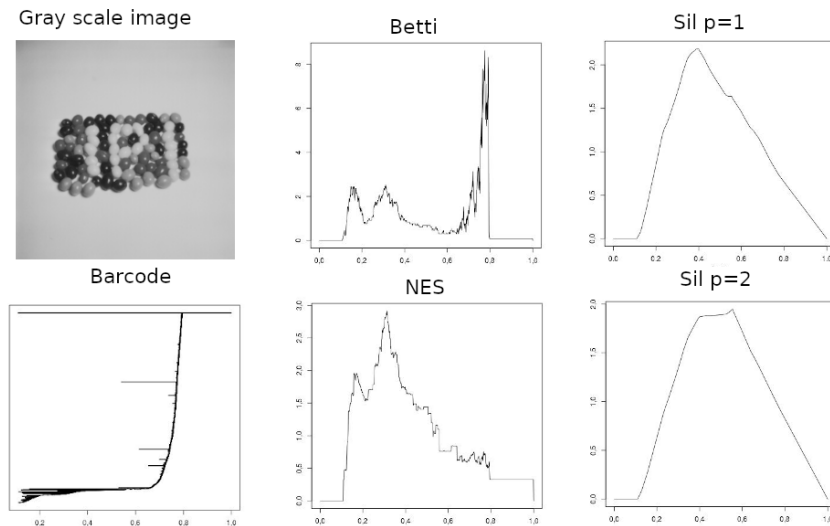


Figure 8: An image producing very different output functions

We have followed this procedure:

- Step 1. Transform the images to gray scale.
- Step 2. Add Gaussian, Poisson and salt-and-pepper noise to the data.

¹³<https://github.com/Cimagroup/New-Summary-Function-For-TDA>

¹⁴<https://scikit-tda.org/>

¹⁵<https://persim.scikit-tda.org/>

¹⁶<https://ripser.scikit-tda.org/>

¹⁷<https://scikit-image.org/>

¹⁸<https://scikit-learn.org/>

¹⁹<https://cran.r-project.org/web/packages/TDA/index.html>

Table 2: Average of the L_1 -distance of the selected summary functions on the 0-th persistence barcodes associated to the images from USC-SIPI Image Database and a noisy version of them. Note that the maximum possible value is 2 since all summary functions used have been normalized.

	Betti curve	NES-function	Silhouette $p = 1$	Silhouette $p = 2$
Gauss	0.198	0.114	0.039	0.024
Poisson	0.245	0.200	0.156	0.086
S&P	0.140	0.296	0.424	0.459

Table 3: Images in the database are quite different to each other so these functions are expected to discriminate them. This table shows the average of the L_1 -distance of the considered summary functions on all the images of the given dataset. Note that the maximum possible value is 2 since all summary functions used have been normalized.

Betti curve	NES-function	Silhouette $p = 1$	Silhouette $p = 2$
0.913	0.672	0.500	0.354

Step 3. Compute persistence diagrams using lower-start filtration.

Step 4. Summarize the diagrams using some vectorization method: the Betti curve, the NES-function or the persistence silhouettes.

Let us compare the results obtained. First, the computational time was very similar to obtain all of them so we have omitted it from the analysis. A first conclusion is that for some images like the one in Figure 7, the outputs have extremely similar shapes while in others, like the one in Figure 8, the outputs have completely different shapes, showing that these functions may provide complementary information regarding different aspects of the same image. Robustness results have been obtained computing the L_1 -distance of each summary function on clean and noisy images, see Table 2. Observe that the results obtained for the NES-function is always between those obtained for the Betti curve and the persistence silhouettes. The Betti curve only performs better for salt-and-pepper noise. This fact is expected since persistence diagrams together with the bottleneck distance are unstable to salt-and-pepper noise when they are calculated using the lower-star filtration. It tells us that the NES-function and the persistence silhouettes are more robust to statistical noise than the Betti curve. However, the Betti curve is more robust to impulsive noise.

We have also pairwise compared all the clean images for each summary function using the L_1 -distance and, as expected, since all images in the database are different in nature, this value is high, see Table 3.

We can conclude that the NES-function is usually more discriminative than the persistence silhouettes but less than the Betti curve. Nevertheless, these functions may provide information regarding different aspects of the same image and therefore may complement each other as it is shown in the next subsection.

5.2 FMD dataset experiment

First, we have transformed the given color images to gray scale images and computed their lower-start filtration. In a first part of this experiment, we have computed the Betti curve, the NES-function and the persistence silhouette for $p = 1$. Materials in the FMD database are classified in ten categories: 0-foilage, 1-glass, 2-leather, 3-metal, 4-paper, 5-plastic, 6-stone, 7-water, 8-wood and 9-fabric. Then, we have applied the random forest technique to classify the images using the output of the summary functions. Results are shown in Table 4. Note that the one that performs best is the combination of the Betti curve and the NES function. Besides, the persistence silhouettes also improve their performance when combined with the NES-function.

Table 4: Accuracy of the classification of the FMD database using the random forest technique and the summary functions selected. Note that both, the Betti curve and the persistence silhouettes improve when combined with the NES-function.

Betti	Silhouette $p = 1$	Nes	B + S	B + N	S + N	B + S + N
0.285	0.185	0.24	0.285	0.29	0.25	0.265

In a second part of this experiment, we want to illustrate that, depending on the data, some methods may perform better than others. This is the reason why this time we do not combine

functions. The idea is to try to distinguish categories in the database when compared pairwise. We have performed 45 tests, one for each pair of materials. We have added another popular vectorization method: persistence images (with 20×20 pixels). Results are shown in Table 5 where best marks have been highlighted.

Table 5: We perform a classification task for each pair of categories in FMD. It can be checked that persistence images and the Betti curve usually performs better but the persistence silhouettes and the NES-function may outperform the Betti curve and the persistence images in some cases, concluding that the information provided by each function are complementary and depend on the data.

	0vs1	0vs2	0vs3	0vs4	0vs5	0vs6	0vs7	0vs8	0vs9
B	0.6	0.675	0.7	0.6	0.575	0.725	0.675	0.8	0.775
S	0.625	0.525	0.55	0.45	0.55	0.75	0.575	0.775	0.675
N	0.5	0.6	0.7	0.5	0.45	0.725	0.7	0.8	0.775
PI	0.55	0.725	0.8	0.675	0.6	0.775	0.875	0.85	0.825
	1vs2	1vs3	1vs4	1vs5	1vs6	1vs7	1vs8	1vs9	2vs3
B	0.8	0.55	0.75	0.75	0.725	0.575	0.65	0.575	0.475
S	0.825	0.65	0.8	0.6	0.75	0.475	0.775	0.6	0.45
N	0.85	0.6	0.775	0.75	0.775	0.625	0.675	0.675	0.5
PI	0.85	0.775	0.775	0.675	0.875	0.575	0.625	0.675	0.6
	2vs4	2vs5	2vs6	2vs7	2vs8	2vs9	3vs4	3vs5	3vs6
B	0.825	0.7	0.7	0.525	0.65	0.65	0.725	0.925	0.825
S	0.725	0.575	0.5	0.5	0.6	0.55	0.675	0.65	0.6
N	0.725	0.65	0.55	0.475	0.65	0.75	0.7	0.85	0.625
PI	0.8	0.8	0.625	0.625	0.575	0.7	0.65	0.775	0.775
	3vs7	3vs8	3vs9	4vs5	4vs6	4vs7	4vs8	4vs9	5vs6
B	0.7	0.625	0.725	0.55	0.825	0.725	0.625	0.55	0.65
S	0.625	0.6	0.675	0.625	0.7	0.65	0.45	0.6	0.6
N	0.7	0.65	0.725	0.55	0.75	0.725	0.6	0.65	0.725
PI	0.6	0.725	0.675	0.625	0.775	0.775	0.65	0.625	0.6
	5vs7	5vs8	5vs9	6vs7	6vs8	6vs9	7vs8	7vs9	8vs9
B	0.85	0.7	0.8	0.9	0.825	0.8	0.875	0.65	0.9
S	0.7	0.7	0.625	0.625	0.675	0.675	0.7	0.7	0.575
N	0.7	0.675	0.675	0.775	0.775	0.725	0.7	0.7	0.625
PI	0.825	0.725	0.55	0.7	0.775	0.675	0.725	0.725	0.625

6 Conclusions and future work

In this paper, the stability of persistent entropy is provided justifying its application as an useful statistic in topological data analysis. What is more, persistent entropy has been used to define an stable summary function, the ES-function, and its normalised version, the NES-function. We have shown that, in general, they perform better than the Betti curve in noisy context and that they can be useful for machine learning tasks.

Several types of persistence curves inspired in our persistent entropy summaries were also defined by Y.M Chung and A. Lawson in [35]. They also corroborate the idea that such persistence functions are somehow complementary and combined provide a classification performance comparable to the state of the art. Together with Y.M. Chung and A. Lawson we plan to apply our summary functions to other higher dimensional non-image dataset such as, for example, the TOSCA dataset of 3D meshes²⁰. Besides, as a future work, it would be interesting to deeply compare these and other summary functions with other topological vectorization methods existing in the literature.

Acknowledgments: We would like to thank the reviewers for their very valuable comments and suggestions. The third author has been partially funded by VI-PPITUS (University of Seville).

References

- [1] M. Mrozek, M. Żelawski, A. Gryglewski, S. Han, and A. Krajniak, “Homological methods for extraction and analysis of linear features in multidimensional images,” *Pattern Recognit.*, vol. 45, no. 1, pp. 285 – 298, 2012.
- [2] S. Biasotti, D. Giorgi, M. Spagnuolo, and B. Falcidieno, “Size functions for comparing 3d models,” *Pattern Recognit.*, vol. 41, no. 9, pp. 2855 – 2873, 2008.

²⁰http://tosca.cs.technion.ac.il/book/resources_data.html

- [3] M. Ferri, “Persistent topology for natural data analysis — a survey,” *Towards Integrative Machine Learning and Knowledge Extraction. Lecture Notes in Computer Science. Springer*, vol. 10344, no. 2, pp. 127–139, 2017.
- [4] G. Carlson, A. Zomorodian, A. Collins, and L. Guibas, “Persistence barcodes for shapes,” *Int. Journal of Shape Modeling*, vol. 11, no. 02, pp. 149–187, 2005.
- [5] H. Edelsbrunner, D. Letscher, and A. Zomorodian, “Topological persistence and simplification,” *Discrete Comput. Geom.*, vol. 28, no. 4, pp. 511–533, 2002.
- [6] P. Bubenik, “Statistical topology using persistence landscapes,” *J. Mach. Learn. Res.*, vol. 16, pp. 77–102, 2015.
- [7] H. Edelsbrunner and J. Harer, *Computational Topology: An Introduction*. American Mathematical Society, 2010.
- [8] N. Otter, M. Porter, U. Tillmann, P. Grindrod, and H. Harrington, “A roadmap for the computation of persistent homology,” *Entropy*, vol. 17, no. 6, 2017.
- [9] Y. Mileyko, S. Mukherjee, and J. Harer, “Probability measures on the space of persistence diagrams,” *Inverse Problems*, vol. 27, no. 12, p. 124007, 2011.
- [10] C. Shannon, “A mathematical theory of communication,” *Bell System Technical Journal*, vol. 27, no. 3, pp. 379–423, 1948.
- [11] M. Rucco, F. Castiglione, E. Merelli, and M. Pettini, “Characterisation of the idiotypic immune network through persistent entropy,” in *Proceedings of ECCS 2014*, pp. 117–128, 2014.
- [12] H. Chintakunta, T. Gentimis, R. Gonzalez-Diaz, M. J. Jimenez, and H. Krim, “An entropy based persistence barcode,” *Pattern Recognit.*, vol. 48, no. 2, pp. 391–401, 2015.
- [13] E. Merelli, M. Piangerelli, M. Rucco, and D. Toller, “A topological approach for multivariate time series characterization: the epileptic brain,” *EAI Endorsed Transactions on Self-Adaptive Systems*, vol. 16, no. 7, 2016.
- [14] M. Rucco, R. Gonzalez-Diaz, M. Jimenez, N. Atienza, and et al, “A new topological entropy-based approach for measuring similarities among piecewise linear functions,” *Signal Process*, vol. 134, pp. 130–138, 2017.
- [15] J. Binchi, E. Merelli, M. Rucco, G. Petri, and F. Vaccarino, “jholes: A tool for understanding biological complex networks via clique weight rank persistent homology,” *Electron. Notes Theor. Comput. Sci.*, vol. 306, pp. 5–18, 2014.
- [16] N. Atienza, L. Escudero, M. Jimenez, and M. Soriano-Trigueros, “Persistent entropy: a scale-invariant topological statistic for analyzing cell arrangements,” *Unpublished*, vol. abs/1902.06467, 2019.
- [17] X. Wang, F. Sohel, M. Bennamoun, Y. Guo, and H. Lei, “Scale space clustering evolution for salient region detection on 3d deformable shapes,” *Pattern Recognit.*, vol. 71, pp. 414 – 427, 2017.
- [18] N. Atienza, R. Gonzalez-Diaz, and M. Rucco, “Persistent entropy for separating topological features from noise in vietoris-rips complexes,” *J. Intell. Inf. Syst.*, vol. 52, no. 3, pp. 637–655, 2019.
- [19] J. Reininghaus, S. Huber, U. Bauer, and R. Kwitt, “A stable multi-scale kernel for topological machine learning,” in *2015 IEEE Conference on Computer Vision and Pattern Recognition (CVPR)*, pp. 4741–4748, 2015.
- [20] G. Kusano, K. Fukumizu, and Y. Hiraoka, “Persistence weighted gaussian kernel for topological data analysis,” in *Proc. of the 33rd Int. Conf. on Machine Learning*, vol. 48, p. 2004–2013, 2016.
- [21] M. Carrière, M. Cuturi, and S. Oudot, “Sliced Wasserstein kernel for persistence diagrams,” in *Proc. of the 34th Int. Conf. on Machine Learning* (D. Precup and Y. W. Teh, eds.), vol. 70, pp. 664–673, 2017.
- [22] F. Chazal, B. Fasy, F. Lecci, A. Rinaldo, and L. Wasserman, “Stochastic convergence of persistence landscapes and silhouettes,” *J. Comput. Geom.*, vol. 6, no. 2, p. 140–161, 2015.
- [23] H. Adams, T. Emerson, M. Kirby, R. Neville, and et al., “Persistence images: A stable vector representation of persistent homology,” *J. Mach. Learn. Res.*, vol. 18, no. 8, pp. 1–35, 2017.
- [24] E. Richardson and M. Werman, “Efficient classification using the euler characteristic,” *Pattern Recognit. Lett.*, vol. 49, pp. 99–106, 2014.
- [25] P. Pranav, H. Edelsbrunner, R. van de Weygaert, G. Vegter, and et al., “The topology of the cosmic web in terms of persistent betti numbers,” *Mon. Not. R. Astron. Soc.*, vol. 465, no. 4, pp. 4281–4310, 2017.

- [26] B. Rieck, F. Sadlo, and H. Leitte, “Topological machine learning with persistence indicator functions,” in *Topological Methods in Data Analysis and Visualization V*, Springer International Publishing, to appear.
- [27] Y. Umeda, “Time series classification via topological data analysis,” *Trans. Japan Soc. Artificial Intelligence*, vol. 32, no. 3, pp. D–G72_1–12, 2017.
- [28] D. Cohen-Steiner, H. Edelsbrunner, J. Harer, and Y. Mileyko, “Lipschitz functions have l_p -stable persistence,” *Found. Comput. Math.*, vol. 10, no. 2, pp. 127–139, 2010.
- [29] F. Chazal, D. Cohen-Steiner, L. Guibas, F. Mémoli, and S. Oudot, “Gromov-hausdorff stable signatures for shapes using persistence,” *Comput. Graphics Forum*, vol. 28, no. 5, p. 1393–1403, 2009.
- [30] G. Dallal, *The Little Handbook of Statistical Practice*. Amazon Digital Services LLC, 2012.
- [31] B. Lesche, “Instabilities of rényi entropies,” *J. Stat. Phys.*, vol. 27, no. 2, pp. 419–422, 1982.
- [32] T. Cover and J. Thomas, *Elements of Information Theory*. Wiley Series in Telecommunications and Signal Processing, 2nd ed., 2006.
- [33] M. Buchet, Y. Hiraoka, and I. Obayashi, “Persistent homology and materials informatics,” in *Nanoinformatics*, pp. 75–95, Springer, Singapore, 2018.
- [34] Y. Chung, C.-S. Hu, A. Lawson, and C. Smyth, “Topological approaches to skin disease image analysis,” in *2018 IEEE Int. Conf. on Big Data*, 2018.
- [35] Y. Chung and A. Lawson, “Persistence curves: A canonical framework for summarizing persistence diagrams,” *Unpublished*, vol. abs/1904.07768, 2019.
- [36] N. Atienza, R. Gonzalez-Diaz, and M. Soriano-Trigueros, “On the stability of persistent entropy and new summary functions for TDA,” *Unpublished*, vol. abs/1803.08304, 2018.
- [37] L. Breiman, “Random forests,” *Mach. Learn.*, vol. 45, p. 5–32, 2001.